A global model of the marine ecosystem for long-term simulations: Sensitivity to ocean mixing, buoyancy forcing, particle sinking, and dissolved organic matter cycling

A. Schmittner,[1,2] A. Oschlies,[3,4] X. Giraud,[5,6] M. Eby,[7] and H. L. Simmons[8]

[1] A new model of the marine ecosystem coupled into a global Earth System Climate Model suitable for long-term (multimillennial timescale) simulations is presented. The model is based on nitrate as the sole limiting nutrient. Prognostic equations for nutrients, phytoplankton, zooplankton, and detritus are solved online in the three-dimensional ocean circulation model component. Experiments with different parameterizations of vertical mixing, including a scheme of tidally driven mixing, changes in buoyancy forcing in the Southern Ocean, different particle sinking velocities, and the inclusion of dissolved organic matter are performed, and the results are compared with observations. The results reemphasize the roles of Southern Ocean freshwater forcing and diapycnal mixing in the low-latitude pycnocline in setting the global deep water circulation and properties. The influence of high mixing in the Southern Ocean as inferred from observations is much more limited. The deep water circulation also has a strong influence on the marine ecosystem and nutrient distributions. We demonstrate that larger values of vertical diffusion lead to a shallower nutricline due to increased upwelling. Export production and nutrient distributions respond sensitively to changes in mixing and to the ratio of particle sinking to remineralization in the upper ocean. The best fits to global measurements of temperature, salinity, deep ocean radiocarbon, mixed layer depth, nutrients, and chlorophyll are obtained for values of vertical mixing in the pycnocline of around $0.2–0.3 \times 10^{-4}$ m^2/s and for e-folding depth for particle remineralization of $100–200$ m. A simple parameterization of dissolved organic matter dynamics increases primary production and nutrient concentrations in the upper ocean and improves chlorophyll distributions in the subtropical gyres but has no discernible influence on particulate export fluxes. Remaining model deficiencies are identified, and strategies for future model improvement are outlined.

[1]Institute of Geosciences, University of Kiel, Kiel, Germany.
[2]Now at College of Oceanic and Atmospheric Sciences, Oregon State University, Corvallis, Oregon, USA.
[3]Institute of Marine Sciences, Kiel, Germany.
[4]Now at School of Ocean and Earth Science, Southampton Oceanography Centre, Southampton, UK.
[5]Max Planck Institute for Biogeochemistry, Jena, Germany.
[6]Now at Research Center on Ocean Margins, University of Bremen, Bremen, Germany.
[7]School of Earth and Ocean Sciences, University of Victoria, Victoria, British Columbia, Canada.
[8]International Arctic Research Center, University of Alaska, Fairbanks, Alaska, USA.

1. Introduction

[2] The marine ecosystem constitutes an important and active component of the global climate system. One of the key ways in which marine ecosystems affect climate is through their influence on atmospheric carbon dioxide (CO_2) concentrations. Production of organic matter through photosynthesis consumes carbon dioxide in the sunlit upper ocean (euphotic zone). Since much of the organic material remineralizes after sinking to deeper levels, biological activity maintains atmospheric CO_2 at lower levels than it would be in the absence of this sinking flux. This process, also known as the biological pump [e.g., *Falkowski et al.*, 2003], strongly determines the distribution and cycling of carbon in the ocean and atmosphere.

[3] Most ocean carbon cycle models presently do not take into account the explicit treatment of photosynthesis,

but rather parameterize primary production by restoring surface nutrient concentrations toward observations (as in the Ocean Carbon Cycle Intercomparison Project (OCMIP))[*Orr et al.*, 2001]. These models are suitable for estimates of anthropogenic carbon uptake, but may be of limited use for transient climate scenarios or paleo climate studies when it is not known how surface nutrients would be expected to change. On the other hand, detailed global models of the marine ecosystem are being developed that include multiple nutrients and different classes of phytoplankton and zooplankton [*Moore et al.*, 2002; *Aumont et al.*, 2003]. Owing to the large number of tracers, these models are computationally expensive, and the increasing number of poorly known ecological parameters are difficult, if not impossible, to constrain by presently available observations [*Denman*, 2003]. Here we attempt to embark on an intermediate path between those two outlined above. Our goal is to construct a global model of the marine carbon cycle suitable for transient multimillennial timescale integrations. As a first step on this path, we integrate a relatively simple model of the marine ecosystem, based on one limiting nutrient into an existing global coupled Earth System Climate Model (ESCM).

[4] One purpose of the present paper is to provide a detailed reference and description of the model and its performance for the present-day climate. We will demonstrate the ability to perform extensive sensitivity studies and long term integrations. Section 2 describes the physical model, its sensitivity to mixing, and buoyancy forcing of the ocean, and section 3 provides a description of the ecosystem model and its sensitivities to ocean mixing, the sinking and remineralization of organic particles, and the cycling of dissolved organic matter. A detailed sensitivity study concerning the influence of the biological parameters will be presented in a separate paper (A. Schmittner and A. Oschlies, A global model of the marine ecosystem for long term simulations: Sensitivity to biological parameters, manuscript in preparation, 2005) (hereinafter referred to as Schmittner and Oschlies, manuscript in preparation, 2005).

2. Physical Models

[5] This section describes the physical model (section 2.1) and its tuning, with a focus on the ocean circulation. Uncertain parameters are varied, and the resulting temperature and salinity distributions are systematically and objectively compared with observations. We examine diapycnal (section 2.2) and isopycnal (section 2.3) mixing, mixing in the Southern Ocean (section 2.4), and surface buoyancy forcing in the Southern Hemisphere (section 2.5) as control parameters. The model in best agreement with the observations will serve as the reference model in the following sections for the simulations including the biology.

2.1. UVic Model

[6] The physical climate model used is the University of Victoria Earth System Climate Model (UVic ESCM). A detailed model description as well as applications to past, present, and future climates is given by *Weaver et al.* [2001]. Here we will only present a brief overview. The oceanic component is a fully three-dimensional nonlinear general

circulation model of the world's oceans [*Pacanowski*, 1995] with isopycnal mixing and a parameterization of the effect of eddy-induced tracer transport [*Gent and McWilliams*, 1990]. For the isopycnal diffusivity $A_I = 2000$ m^2 s^{-1}, for the thickness diffusion 1000 m^2 s^{-1} is used, and maximum slopes of 0.01 for isopycnal surfaces are allowed. Nineteen levels are resolved in the vertical with varying resolution from 50 m near the surface to 500 m at the seafloor. The flux corrected scheme of *Gerdes et al.* [1991] is applied for tracer advection. A convective adjustment scheme removes vertical instabilities through instantaneous mixing. The ocean module is coupled to a single level energy-moisture balance model of the atmosphere and a dynamic-thermodynamic sea ice component. All model components use a common horizontal resolution of $1.8° \times 3.6°$. The seasonal cycle is resolved; however, the model excites neither higher (weather) nor lower (interannual or longer) frequency variability.

[7] A key process determining the global deep water formation rates and patterns is the surface freshwater forcing and its main control: the atmospheric hydrological cycle. In the UVic ESCM the horizontal moisture transport in the atmosphere is parameterized through a combination of advection (with prescribed seasonally varying winds) and diffusion. The diffusion component represents the action of transient eddies, which are mainly active at mid latitudes. *Saenko et al.* [2003] have recently shown that changes in the meridional water vapor transport in the Southern Hemisphere have a strong influence on global deep water formation through altering the densities of Antarctic Intermediate Water and Antarctic Bottom Water (AABW). They have demonstrated that in conjunction with a parameterization of tidal mixing in the ocean (with small values of diapycnal mixing in the pycnocline), increasing the eddy diffusivity μ for atmospheric moisture transport in the midlatitude Southern Hemisphere leads to an improved simulation of the meridional freshwater fluxes. Here we follow *Saenko et al.* [2003] and, together with a parameterization of tidal mixing (explained in the following subsection), use

$$\mu = \mu_b + f_q \sin(2\phi) \times 10^6 \text{m}^2\text{s}^{-1}, \qquad (1)$$

with a background diffusivity of $\mu_b = 10^6$ m^2 s^{-1}. Here f_q is the parameter which determines the increase at mid-southern latitudes (ϕ is latitude) and in our sensitivity experiments varies between 0 and 2. Higher values of the eddy diffusivity at midlatitudes are justified since the activity of transient eddies is strongest there. Nevertheless the exact value of μ is not well known, for which reason we perform sensitivity experiments varying f_q.

2.2. Diapycnal Mixing

[8] For diapycnal mixing in the ocean the standard UVic model [*Weaver et al.*, 2001] uses horizontally constant profiles of vertical diffusion K$_v$ (0.3×10^{-4} m^2 s^{-1} was added to the values of *Bryan and Lewis* [1979]) ranging from 0.6×10^{-4} m^2 s^{-1} at the surface to 1.6×10^{-4} m^2 s^{-1} at 5000 m depth (experiment K$_v = 0.6$–1.6; see Figure 1). The value of diapycnal mixing is subject to debate in the current oceanographic literature. While direct measurements
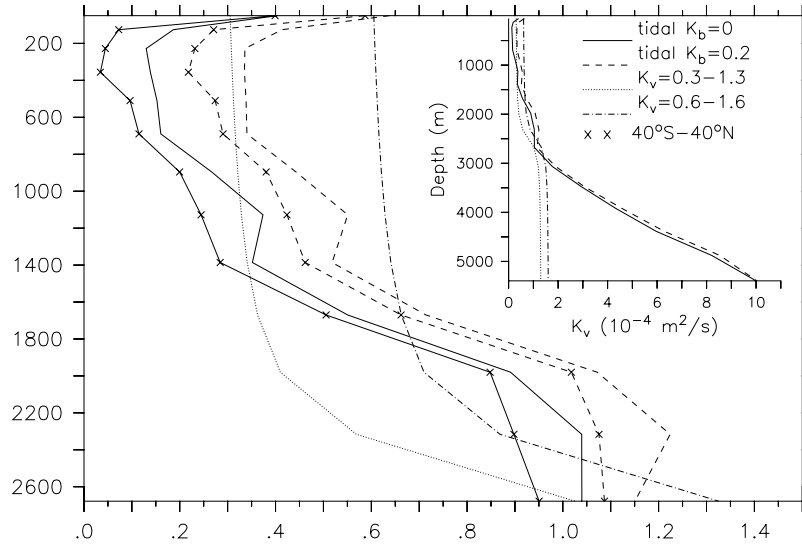
Figure 1. Horizontally averaged profiles of diapycnal mixing.

from open ocean tracer release experiments suggest small values around 0.1×10^{-4} m^2 s^{-1} in the subtropical pycnocline [*Ledwell et al.*, 1994], estimates from inverse modeling using global hydrographic data [*Ganachaud and Wunsch*, 2000] and tracer budgets as well as observations of internal wave velocity fluctuations from the Southern Ocean [*Heywood et al.*, 2002; *Naveira-Garabato et al.*, 2004] yield an order of magnitude higher values for abyssal and

deep waters. In order to consider this large uncertainty, additional experiments were performed (Table 1). In experiment $K_v = 0.3-1.3$, K_v was reduced by a constant offset of 0.3×10^{-4} m^2 s^{-1} yielding back the original values of *Bryan and Lewis* [1979]. Note that the models with constant profiles of vertical mixing ($K_v = 0.3-1.3$ and $K_v = 0.6-1.6$) do not use enhanced Southern Hemisphere moisture transport, such that $f_q = 0$ and $\mu = \mu_b$ in equation (1).

Table 1. Sensitivity Experiments[a]

Experiment Number	Value of Changed Parameter	f_q	NADW, Sv	AABW, Sv	Low Latitude Upwelling,[b] Sv	Primary Production, Gt C yr^{-1}	Export Production,[c] Gt C yr^{-1}	Global ef-Ratio
NA	Observations					36–57[d]	3–16[e]	0.34
1	tidal $K_b = 0$	1	8.4	7.7	2.3	9.2	3.1	0.34
2	tidal $K_b = 0.2$	1	15.8	5.4	7.9	20.7	7.1	0.34
3	tidal $K_b = 0.2$ $\sigma_{DOM} = 0.15, \mu_{DOM} = 0.5$	1	15.8	5.4	7.9	24.6	7.2	0.29
4	tidal $K_b = 0.2$ $\sigma_{DOM} = 0.15, \mu_{DOM} = 0.17$	1	15.8	5.4	7.9	24.0	7.1	0.29
5	tidal $K_b = 0.2$ $\sigma_{DOM} = 0.25, \mu_{DOM} = 0.5$	1	15.8	5.4	7.9	27.0	7.0	0.25
6	tidal $K_b = 0.2$ $\sigma_{DOM} = 0.25, \mu_{DOM} = 0.17$	1	15.8	5.4	7.9	25.2	6.5	0.26
7	tidal $K_b = 0.2$ $A_I = 1000$	1	16.7	5.3	8.1	22.9	8.1	0.35
8	REF (tidal $K_b = 0.2$, $K_v(SO) = 1$)	2	17.2	2.8	6.7	24.1	8.2	0.34
9	$K_v = 0.3-1.3$ $w_D = 5$	0	14.8	7.4	9.4	30.9	9.1	0.29
10	$K_v = 0.3-1.3$ $w_D = 10$	0	14.8	7.4	9.4	16.8	7.0	0.42
11	$K_v = 0.3-1.3$ $w_D = 5-50$	0	14.8	7.4	9.4	30.9	7.1	0.23
12	$K_v = 0.6-1.6$	0	19.0	7.1	14.8	45.2	15.5	0.34
13	$K_v = 0.6-1.6$ $w_D = 3.5$	0	19.0	7.1	14.8	65.3	17.7	0.27

[a]NADW denotes the maximum stream function in the North Atlantic below 300 m and AABW the minimum stream function in the Southern Ocean.
[b]Across 1000 m between 20°S and 20°N.
[c]Through sinking of detritus across 126 m.
[d]*Antoine et al.* [1996], *Morel and Antoine* [2002], *Falkowski et al.* [2003], and *Gregg et al.* [2003].
[e]*Oschlies* [2001].

[9] One important process leading to mixing in the ocean is the dissipation of tidal energy over rough topography. We explicitly include this process using the tidal mixing scheme of *St. Laurent et al.* [2002], as implemented by *Simmons et al.* [2004]. This parameterization uses a map of internal wave energy flux [*Jayne and St. Laurent*, 2001] to estimate the global distribution of tidal energy available for mixing. A stability dependent relation for the vertical diffusivity is formulated for regions where internal tides dissipate their energy as turbulence. Mixing due to tidal energy dissipation is added onto a constant background diffusivity K_b leading to spatially varying diffusivities that resemble observed abyssal mixing rates [*St. Laurent et al.*, 2002]. A previous study using an ocean-only model with restoring boundary conditions [*Simmons et al.*, 2004] demonstrated the impact of this parameterization on simulated water mass structure. Here we use $K_b = 0.2 \times 10^{-4}$ m^2 s^{-1} (experiment tidal $K_b = 0.2$) which produces mean values of K_v around $0.2-0.3 \times 10^{-4}$ m^2 s^{-1} in the low-latitude pycnocline and $K_b = 0$ which leads to very small values of K_v around 0.05×10^{-4} m^2 s^{-1} in the low-latitude pycnocline (see Figure 1). Note that the models with tidal mixing (tidal $K_b = 0.2$ and tidal $K_b = 0$) use increased water vapor flux in the Southern Hemisphere with $f_q = 1$ in equation (1) since otherwise they would have too little deep water formation.

[10] Vertical mixing in the low-latitude pycnocline governs the amount of deep water upwelling to the low-latitude surface [*Gnanadesikan et al.*, 2002]. This is confirmed in our model (Table 1) as well as the effect of K_v on deep water formation in the North Atlantic [*Bryan*, 1987]. Models $K_v = 0.3-1.3$ and tidal $K_b = 0.2$ which have similar values of vertical mixing in the pycnocline also display similar circulations. Vertical diffusion in our model is not dominated by numerical diffusion as lowering K_v to values below 0.2×10^{-4} m^2 s^{-1} still has a strong influence on the circulation.

[11] Global measures of model performance can be inferred from the Taylor diagrams (Figure 2). The simulated distributions of temperature and salinity of models tidal $K_b = 0.2$ and $K_v = 0.6-1.6$ are superior to the other two runs. Model tidal $K_b = 0$ is clearly worst, particularly for salinity. It is interesting to note that despite similar values of pycnocline diffusion and similar circulation patterns, models $K_v = 0.3-1.3$ and tidal $K_b = 0.2$ differ in the salinity simulation. Model $K_v = 0.3-1.3$ shows too salty AABW and too fresh surface waters which is improved in model tidal $K_b = 0.2$ due to the increased poleward water transport in the southern atmosphere. Models tidal $K_b = 0.2$ and $K_v = 0.6-1.6$ display a similar good performance despite large differences in vertical mixing and circulation. Model tidal $K_b = 0.2$ is superior to $K_v = 0.6-1.6$ in the temperature distribution for all three global measures. For the salinity distribution, tidal $K_b = 0.2$ clearly shows better agreement with the observed variance, whereas the correlation is slightly less and pattern RMS error is about the same. The similar performance clearly demonstrates that through a combination of changes in vertical mixing and surface bouyancy fluxes (in our case freshwater flux in the Southern Ocean), it is possible to achieve agreement with the observed temperature and salinity distributions for very different values of diapycnal mixing in the pycnocline. Thus
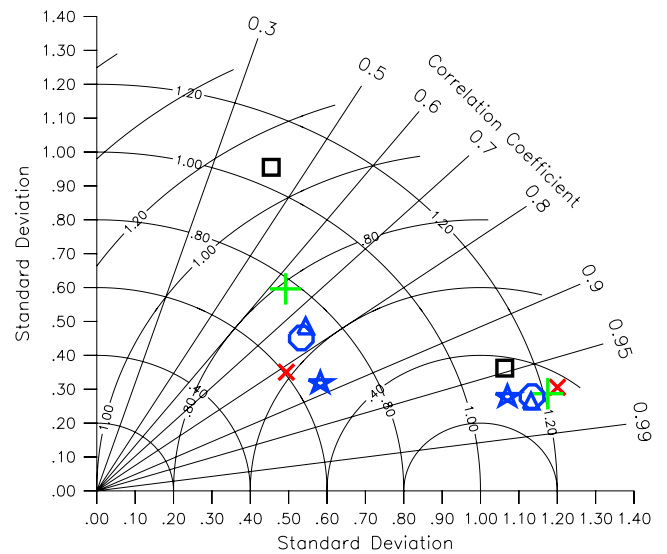

Figure 2. *Taylor* [2001] diagram of model performance for annual mean potential temperature (symbols at bottom right) and salinity (in the left part) distributions with respect to observations [*Levitus et al.*, 1994; *Levitus and Boyer*, 1994]. Black square, tidal $K_b = 0$; blue circle, tidal $K_b = 0.2$; blue triangle base down, tidal $K_b = 0.2$ $A_I = 1000$; blue star, REF; green plus, $K_v = 0.3-1.3$; red cross, $K_v = 0.6-1.6$. All values have been normalized with the standard deviation of the observations. The diagram is easy to read: The standard deviation of a simulation is the distance to the origin. The correlation with the observations can be inferred from the azimuthal position, as indicated by the straight lines converging at the origin, and the pattern RMS difference (that is the RMS difference without the global average) is denoted by the isolines centered around (1,0). Thus a simulation in perfect agreement with the observations would plot on the x-axis at standard deviation 1, correlation 1, and RMS error zero.

temperature and salinity distributions alone do not provide good constraints on the value of diapycnal mixing.

2.3. Isopycnal Mixing

[12] In order to test the influence of changes in along-isopycnal mixing, experiment tidal $K_b = 0.2$ was repeated with reduced diffusivity $A_I = 1000$ m^2 s^{-1} and is labeled tidal $K_b = 0.2$ $A_I = 1000$. Reducing A_I leads to a slightly worse simulation of the salinity distribution and a slight improvement of the simulated temperature patterns. The relatively small changes imply that the temperature and salinity distributions are, in this range, much less sensitive to changes in isopycnal mixing compared to changes in diapycnal mixing.

2.4. Southern Ocean Mixing

[13] Of the above discussed simulations, model tidal $K_b = 0.2$ appears to be in best agreement with the observations. Nevertheless, all models display a cold bias in the deep ocean, and the models with low or intermediate diffusivities
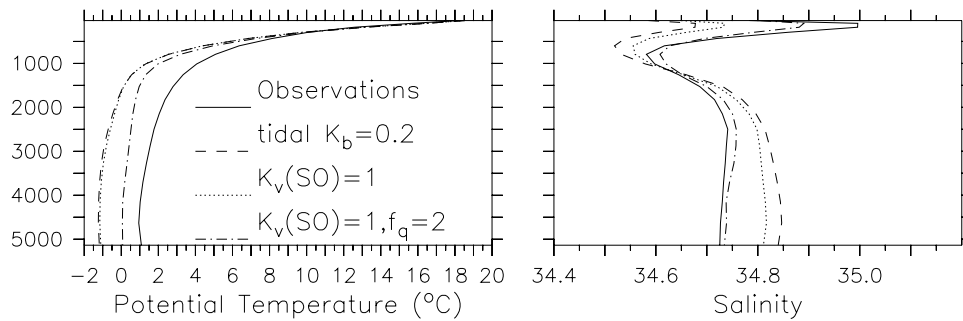
Figure 3. Global horizontally averaged profiles of potential temperature and salinity for selected experiments. Observations [*Levitus et al.*, 1994; *Levitus and Boyer*, 1994] are shown as solid line.

also suffer from a salinification of the deep ocean whereas the upper ocean becomes too fresh. The global mean temperature bias is least for model $K_v = 0.6-1.6$ ($-1.3°C$) and increases to $-2.2°C$ for models $K_v = 0.3-1.3$ and tidal $K_b = 0.2$ and is worse ($-3.3°C$) for tidal $K_b = 0$. Additional analysis (not shown) reveals that the salinification of bottom waters in the low and intermediate diffusivity models originates from the Southern Ocean. Cold and salty water masses are produced through brine rejection during sea ice formation on the Antarctic shelf regions and subsequently propagate down the continental slope. We hypothesize that too little mixing with surrounding water masses might be the reason for the biases in the low and intermediate mixing cases. Moreover, recent observations of vertical diffusivities in the Southern Ocean indicate high values below about 500 m of more than $1 \times 10^{-4} \text{ m}^2 \text{ s}^{-1}$ [*Naveira-Garabato et al.*, 2004]. An additional experiment was therefore performed in which the vertical diffusivity was increased to $1 \times 10^{-4} \text{ m}^2 \text{ s}^{-1}$ below 500 m depth and southward of 50°S. As shown in Figure 3 (experiment $K_v(SO) = 1$) this improves the salinity bias somewhat but has no discernible influence on the temperature distribution. This result demonstrates the limited effect of the observed high diapycnal mixing in the deep Southern Ocean on deep water hydrography and circulation. The effect of high diapycnal mixing which extends to the surface seems to have a larger effect on radiocarbon and oxygen [*Gnanadesikan et al.*, 2004].

2.5. Southern Ocean Freshwater Budget

[14] All models described above experience a systematic bias in water mass distributions. The southward propagation of NADW is too shallow and AABW fills too large volumes of the deep Atlantic. As previously shown by *Saenko et al.* [2003] Southern Ocean meridional freshwater transports can be improved by increasing the southward atmospheric moisture transport in the Southern Hemisphere, which also improves global water mass distributions. We adopt this strategy and increase f_q in equation (1) from 1 to 2. Comparison with NCAR/NCEP reanalysis data shows improved simulation of precipitation in the Southern Hemisphere (not shown). The effect on deep water mass properties is remarkable (Figure 3, experiment $K_v(SO) = 1, f_q = 2$). The deep salty bias is completely

removed, and globally averaged salinity profiles are now in excellent agreement with observations. Freshening of high-latitude surface waters in the areas of AABW formation decreases the density and production rate (minimum stream function south of 60°S decreases from -7.0 Sv to -3.2 Sv) of AABW. NADW occupies deeper levels, and although its total production rate increased only by 1.4 Sv (Table 1) the export to the Southern Ocean (calculated as maximum stream function in the Atlantic at 35°S) increased by 2.8 Sv from 11.8 Sv to 14.6 Sv. Both decreased influence of AABW and increased import of NADW warms global deep waters by about 1°C decreasing the global temperature bias from $-2.2°C$ to $-1.2°C$. This result demonstrates the importance of freshwater forcing in the Southern Ocean on global deep water properties. This model version (hereinafter called REF) also shows the best performance in the global measures shown in the Taylor diagram (Figure 2), although a slight deep cold bias remains (Figure 3).

2.6. Deep Ocean Ventilation

[15] As mentioned before, temperature and salinity distributions alone do not provide good constraints on the values of diapycnal mixing. A variable which responds more sensitively to diapycnal mixing is radiocarbon ($\Delta^{14}C$). Figure 4 shows that the reference model agrees relatively well with observed concentrations of radiocarbon in the deep ocean. The progressive aging of NADW along its way south and into the other basins is reproduced by the model. Youngest waters at 3 km depth are found in the North Atlantic with $\Delta^{14}C$ values between -60 and -100 permil, oldest waters in the North Pacific of up to -300 permil, and intermediate values in the Indian and Southern Ocean. Deep waters in the Southern Ocean are 20 permil too old, and in the North Pacific they are up to 40 permil older than the observations. As such, the model lies within the error bars of the observations using the metric (their Figure 2) of *Matsumoto et al.* [2004] for North Atlantic and Circumpolar deep water whereas North Pacific Deep Water is slightly too old in the model. This suggests that vertical diffusivities might be slightly too low in the reference model. Models with still lower diffusivities lead to even older (lower $\Delta^{14}C$) waters in the North Pacific, and higher diffusivities produce too young deep waters (not shown)
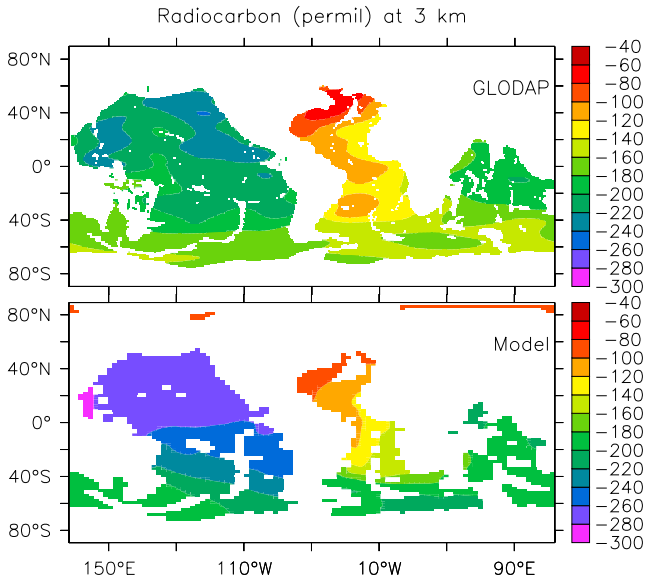
Figure 4. (bottom) Radiocarbon at 3 km depth for the reference model REF after 4000 years of integration together with (top) observations from the Global Ocean Data Analysis Project (GLODAP, http://cdiac3.ornl.gov).

confirming the early studies by *Toggweiler et al.* [1989] and *Gnanadesikan et al.* [2004].

2.7. Mixed Layer Depths

[16] A physical variable particularly important for the simulation of the marine ecosystem is the mixed layer depth as it controls the depth from which nutrients are supplied to the surface. Figure 5 shows that the model captures the main features of maximum (winter) mixed layer depths in the observations. In the tropics, mixed layer depths are around 50 m with minimum values in the eastern and western basins of the Atlantic and Pacific oceans and higher values in the center of these basins and in the Arabian sea. Generally, mixed layer depths increase toward higher latitudes. Maximum values are observed in the eastern Indian and in the Pacific sector of the Southern Ocean between about 40°S and 60°S, in the Weddell Sea with an extension toward the east, in the Ross Sea, and in the northern North Atlantic. The only major model bias is the too shallow mixed layer depth in the Nordic Seas. This is caused by a well-known cold bias and excessive sea ice cover there [*Weaver et al.*, 2001].

3. Biological Model

[17] This section describes the ecosystem model (section 3.1) and chlorophyll and nutrient distributions obtained with the reference model (section 3.2), as well as sensitivities to mixing (section 3.3), particulate organic matter (section 3.4), and dissolved organic matter (section 3.5) fluxes.

3.1. Model Description

[18] We use an ecosystem model of nitrogen cycling which is based to a large extent on previous studies by

Sarmiento et al. [1993] and *Six and Maier-Reimer* [1996]. Originally, the model has been set up for the North Atlantic [*Oschlies and Garçon*, 1999], where nitrate can, to a good approximation, be regarded as the limiting nutrient and where limitation by iron is not assumed to be active. Given our current views about significant controls and functions of ecosystems, the model clearly is oversimplified. For example, it does not explicitly account for iron limitation, nitrogen fixation, denitrification, non-Redfield dissolved-organic matter dynamics, or different functional phytoplankton groups. Neither does it explicitly resolve the short-lived nutrient pool of ammonia. The model uses a very simple formulation of particle sinking with horizontally and temporally uniform sinking velocities. In contrast, previous global model simulations in general employed instantaneous sinking and remineralization according to a prescribed remineralization profile [*Suess*, 1980; *Martin et al.*, 1987; *Orr et al.*, 2001].

[19] The ecosystem model (Figure 6) is adapted from *Oschlies and Garçon* [1999] and will be reviewed briefly below. It consists of five prognostic variables: nutrients (N), phytoplankton (P), zooplankton (Z), particulate detritus (D), and dissolved organic matter (DOM), all expressed in units of mmol nitrogen per m^3. Each variable changes its concentration C according to the following equation:

$$\frac{\partial C}{\partial t} = T + S, \qquad (2)$$

where T represents all transport terms including advection, isopycnal and diapycnal diffusion, and convection. S
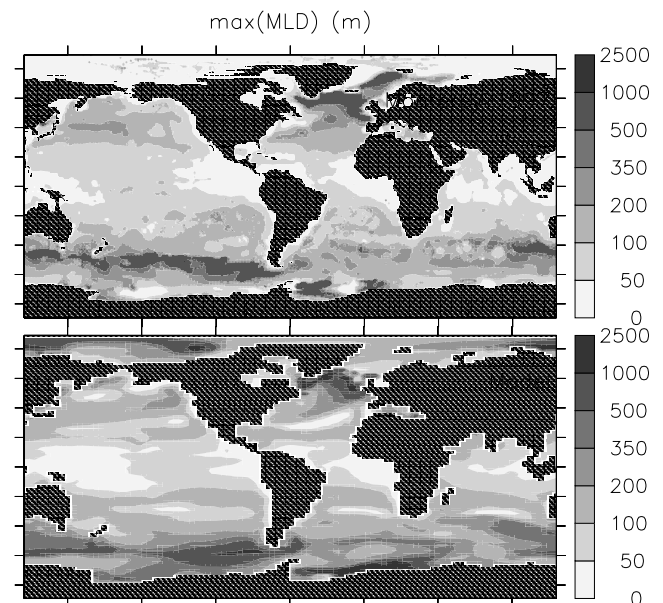

Figure 5. Maximum of monthly mixed layer depths. (top) Observations from *Monterey and Levitus* [1997]. (bottom) Simulated mixed layer depth (model REF) calculated using a density criterion of $\Delta\sigma_\theta = 0.15$ kg/m^3.
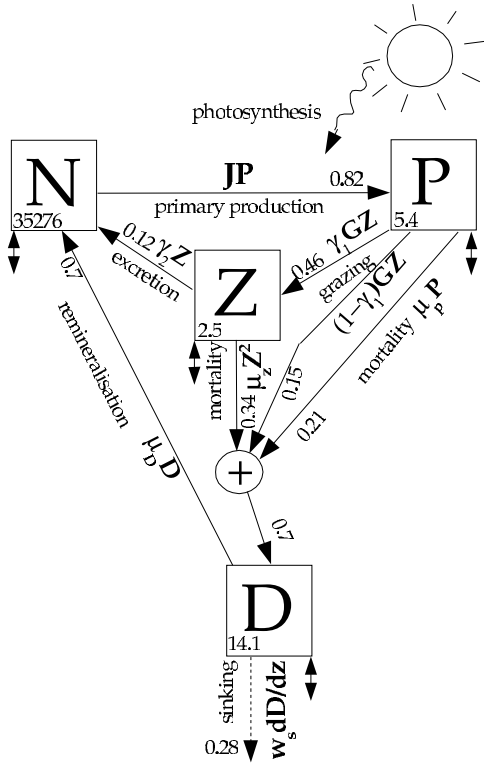
Figure 6. Compartments and interactions of the ecosystem model. Solid one-sided arrows represent fluxes between the compartments. The double-sided arrows denote that each biological tracer is also influenced by the circulation. An additional transport term through sinking of detritus is indicated by the dashed arrow. See text for further description. Also given are global (numbers in lower left corners) inventories (10^{15} mmol N) and global fluxes (10^{15} mmol N d^{-1}; to convert to GtC/yr multiply by 2.9×10^{-14}) at year 2000 of model REF. The value for the sinking of detritus is evaluated at 126 m.

denotes the source minus sink terms, which describe the biological interactions as follows:

$$S(\mathrm{N}) = \mu_D \mathrm{D} + \mu_{DOM}\mathrm{DOM} + \gamma_2 Z - J(I,\mathrm{N})\mathrm{P}, \qquad (3)$$

$$S(\mathrm{P}) = J(I,\mathrm{N})\mathrm{P} - G(\mathrm{P})Z - \mu_P \mathrm{P}, \qquad (4)$$

$$S(Z) = \gamma_1 G(\mathrm{P})Z - \gamma_2 Z - \mu_Z Z^2, \qquad (5)$$

$$S(\mathrm{D}) = (1 - \sigma_{DOM})\big((1 - \gamma_1)G(\mathrm{P})Z + \mu_P \mathrm{P} + \mu_Z Z^2\big) - \mu_D \mathrm{D} \\ - w_D \frac{\partial \mathrm{D}}{\partial z}, \qquad (6)$$

$$S(\mathrm{DOM}) = \sigma_{DOM}\big((1 - \gamma_1)G(\mathrm{P})Z + \mu_P \mathrm{P} + \mu_Z Z^2\big) - \mu_{DOM}\mathrm{DOM}, \qquad (7)$$

where J is the phytoplankton growth rate and G is the grazing function. The remaining parameters are described in

Table 2. The equations are solved in the entire model domain extending to the seafloor.

[20] The growth rate of phytoplankton is limited by irradiance (I) and nutrients (N),

$$J(I,\mathrm{N}) = \min\left(J_I, J_{\max}\frac{N}{k_1 + N}\right), \qquad (8)$$

where J_I denotes the purely light-limited growth rate, and $J_{\max}$ is the light-saturated growth

$$J_{\max} = ab^{cT}, \qquad (9)$$

which depends only on temperature T (°C). The light-limited growth is calculated according to

$$J_I = \frac{J_{\max}\alpha I}{\left[J_{\max}^2 + (\alpha I)^2\right]^{1/2}}, \qquad (10)$$

where α is the initial slope of the photosynthesis versus irradiance (P-I) curve and

$$I = I_{z=0}\ \mathrm{PAR}\ e^{-k_w \tilde{z} - k_c \int_0^{\tilde{z}} \mathrm{P}dz} \\ \cdot \left[1 + a_i\left(e^{-k_i(h_i + h_s)} - 1\right)\right] \qquad (11)$$

is the shortwave radiation at depth z. Here $I_{z=0}$ denotes the downward shortwave radiation at the sea surface calculated by the atmospheric model component, and $\tilde{z} = z/\cos\theta_o = z/\sqrt{1 - \sin^2\theta/1.33^2}$ is the effective vertical coordinate (positive downward), with $\frac{\sin\theta}{\sin\theta_o} = 1.33$ as the refraction index according to Snell's law relating the angle of incidence in air θ to the angle of incidence in water θ_o. The term in the brackets of equation (11) describes attenuation of light through sea ice of height h_i and possible snow cover of height h_s, where a_i is the fractional sea ice cover. The angle of incidence $\theta = \phi - \delta$ is a function of latitude ϕ and the declination

$$\delta = \varepsilon\frac{\pi}{180°}\sin[(f - 0.22)2\pi], \qquad (12)$$

where f is the fraction of year. At the equinoxes on 21 March ($f = 0.22$) and 21 September, $\theta = \phi$, and at summer (winter) solstice it is at its minimum (maximum) $\phi \pm \varepsilon$, with Earth's obliquity $\varepsilon = 23°$ for the present orbital configuration.

[21] Equation (10) is averaged over depth and a triangular shaped diurnal cycle using the method of *Evans and Parslow* [1985]. Total growth becomes

$$J_I^{ave} = \frac{1}{\Delta z \cdot 24h}\int_{z - \frac{\Delta z}{2}}^{z + \frac{\Delta z}{2}}\int_{0h}^{24h} J_I dz dt \\ = \frac{G_D}{k_w \Delta z}\left[\Phi\left(\frac{2G_I}{G_D}\right) - \Phi\left(\frac{2G_I}{G_D}e^{-(k_w + k_c \mathrm{P})\Delta z}\right)\right], \qquad (13)$$

where Δz is the layer depth. The light saturated growth in a day of fractional day length $d = \arccos(-\tan\phi\tan\delta)/\pi$ is $G_d = J_{\max}d$, and at low light growth is in the linear range

Table 2. Ecosystem Model Parameters

Parameter	Symbol	Value	Units
Phytoplankton (P) Coefficients			
Initial slope of P-I curve	α	0.025	$(W\ m^{-2})^{-1}\ d^{-1}$
Photosynthetically active radiation	PAR	0.43	
Light attenuation in water	k_w	0.04	m^{-1}
Light attenuation through phytoplankton	k_c	0.03	$m^{-1}(mmol\ m^{-3})^{-1}$
Light attenuation through sea ice[a]	k_i	5	m^{-1}
Maximum growth rate parameters	a	0.6	d^{-1}
	b	1.066	
	c	1.0	$(°C)^{-1}$
Half-saturation constant for N uptake	k_1	0.5	$mmol\ m^{-3}$
Specific mortality rate	μ_P	0.03	d^{-1}
Zooplankton (Z) Coefficients			
Assimilation efficiency	γ_1	0.75	
Maximum grazing rate	g	2.0	d^{-1}
Prey capture rate	ϵ	1.0	$(mmol\ m^{-3})^{-2}d^{-1}$
Mortality	μ_Z	0.2	$(mmol\ m^{-3})^{-2}d^{-1}$
Excretion	γ_2	0.03	d^{-1}
Detritus (D) Coefficients			
Remineralization rate	μ_D	0.05	d^{-1}
Sinking speed	w_D	5[b]	$m\ d^{-1}$
Dissolved Organic Matter (DOM) Coefficients			
Production ratio	σ_{DOM}	0.15[b]	
Remineralization rate	μ_{DOM}	0.17[b]	yr^{-1}

[a]Value in the center of range reported by *Shirasawa et al.* [2001].
[b]Variable (see text).

$G_I = \alpha I|_{z-\Delta z/2}$ where the radiation I is evaluated at the top of the layer $z - \Delta z/2$. The function $\Phi(u) = \ln(u + \sqrt{1 + u^2}) - \frac{\sqrt{1+u^2}-1}{u}$ is approximated by $\Phi(u) = \frac{0.555588u+0.004926u^2}{1+0.88721u}$ as recommended by *Evans and Garçon* [1995]. The grazing function is taken as

$$G(P) = \frac{g\epsilon P^2}{g + \epsilon P^2}, \qquad (14)$$

with the parameters given in Table 2.

[22] Two types of detritus are considered. Particulate organic detritus sinks to deeper levels with speed w_D and remineralizes with a fast rate μ_D, whereas dissolved organic matter does not sink and remineralizes more slowly. The value of σ_{DOM} determines the relative production. For $\sigma_{DOM} = 0$, no dissolved organic matter is produced.

[23] Initial tests showed that the biology model converges for time steps of $\Delta t \simeq 3$ hours using Euler forward integration. In order to avoid negative concentrations, outgoing fluxes in equations (3)–(6) are set to zero whenever a tracer falls below a minimum concentration of 10^{-12} mmol N/m^3. Nevertheless, small negative values occur during the integration due to the advection and diffusion schemes. However, total nitrate is exactly conserved.

[24] We start the model from rest with zonally averaged values of potential temperature and uniform salinity. Initial nutrient values are set to 5 mmol m^{-3} at the surface and 29.5 mmol m^{-3} elsewhere. This ensures that the total nitrate content in the model is the same as in the observations [*Conkright et al.*, 1998]. Phytoplankton and zooplankton are initialized using exponential profiles with 0.14 mmol m^{-3} and 0.014 mmol m^{-3}, respectively, at the

surface and an e-folding depth of 100 m. For detritus a uniform start value of 10^{-4} mmol m^{-3} is used and DOM is initialized with zero everywhere. The coupled ecosystem-circulation model is integrated for 2000 years until an approximately steady seasonally cycling state is reached.

3.2. Annual Mean Distributions of Biota and Nutrients

[25] The global distribution of phytoplankton expressed as chlorophyll *a* concentrations simulated by the reference model (REF) is roughly consistent with satellite observations (Figure 7). Clearly visible as areas of low chlorophyll concentrations are the centers of the oligotrophic subtropical gyres. Elevated chlorophyll levels in the tropical upwelling regions and the high-latitude areas of strong seasonal mixed layer dynamics are also well represented, indicating more intense biological activity. Main systematic differences are an underestimation of phytoplankton at high northern latitudes and in the centers of the subtropical gyres, and too large concentrations in the Southern Ocean between 40°S and 60°S. Satellite-derived chlorophyll estimates are still associated with considerable uncertainties caused by biases in very oligotrophic and very eutrophic conditions, by systematic overestimation of chlorophyll concentrations in near coastal areas and at high latitudes.

[26] Insufficient oceanic heat transport to the Nordic Seas and into the Arctic, a known model bias [*Weaver et al.*, 2001], and associated too shallow winter mixed layers (Figure 5) as well as overestimated sea ice cover are presumably the main reasons for the too low simulated chlorophyll concentrations there. The Southern Ocean and tropical eastern Pacific are areas where in the real world, limitation of biological productivity by iron is thought to
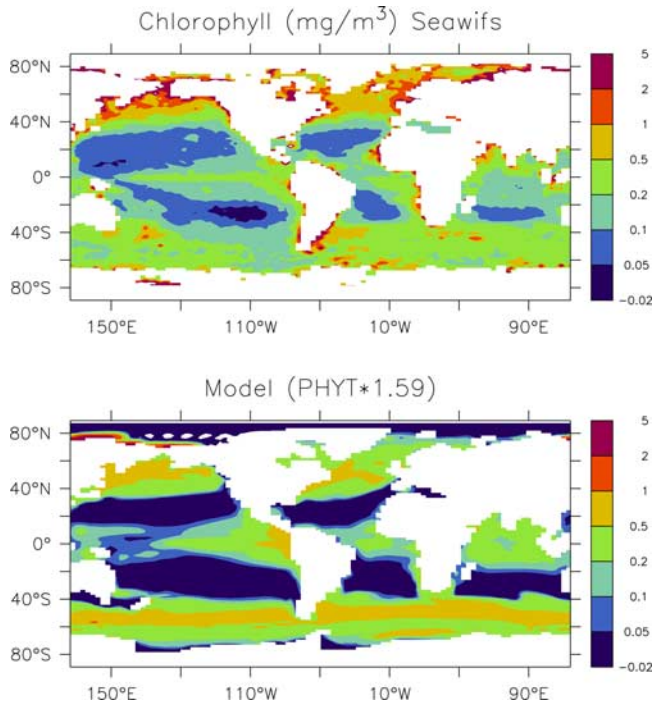
Figure 7. Annual mean distribution of chlorophyll a (mg m^{-3}) (top) as estimated from the Sea-viewing Wide Field-of-view Sensor (SeaWiFS) satellite observations [*Halpern et al.*, 2003] from 1998 to 2002 and (bottom) as simulated by model REF. Observations were interpolated onto the model grid. The modeled phytoplankton concentration in the surface layer was multiplied by 1.59 to convert from mmol N to mg chlorophyll.

the meridional gradient is too sharp and shifted too far south. The discrepancies north of 55°S can be improved by using a lower maximum growth rate for phytoplankton (Schmittner and Oschlies, manuscript in preparation, 2005). The discrepancies at high southern latitudes might be caused by underestimated productivity in the model, too high mixing, a summer bias in the observations, or a combination of these factors.

[29] The reference simulation (REF) also captures the main features of the observed depth distribution of nitrate (Figure 9). Clearly visible is the southward propagation of low nutrient NADW. Highest nutrient concentrations are found in the North Pacific, indicating old and poorly ventilated water masses. The simulated maximum does not extend as deep as in the observations, presumably owing to too little sinking of detritus to the deep ocean. This might be improved in the future with a more realistic parameterization of particle sinking, for example, by increasing the sinking speed with depth, a depth or temperature dependent remineralization rate or a more sophisticated model taking into account aggregate formation [e.g., *Ruiz et al.*, 2002]. Nutrient levels in the upper 1 km of the Southern Ocean are somewhat overestimated despite the neglect of iron limitation. Underestimated lateral export is not likely to be the cause since decreasing isopycnal diffusion did not affect nutrient concentrations in the Southern Ocean much. The maximum is less pronounced in the simulations with weaker stratification of high-latitude waters ($f_q = 0 - 1$). We therefore think that this feature might be related to a combination of high
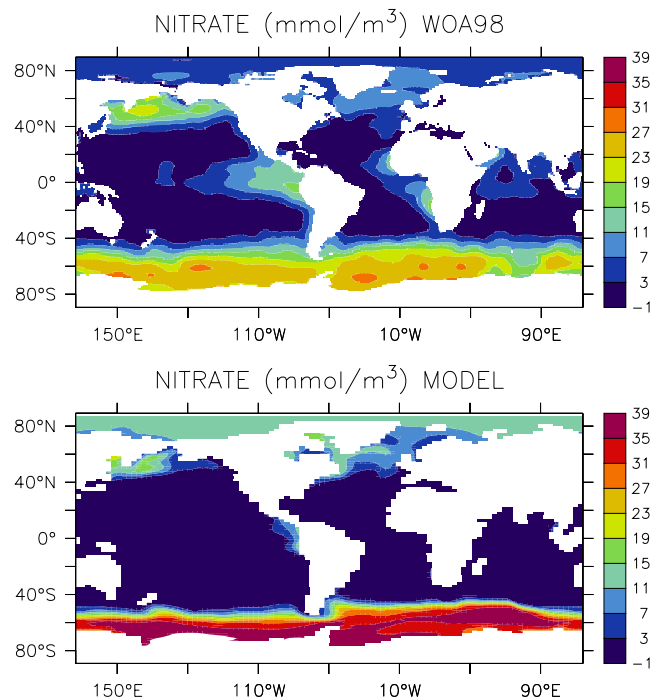
play a significant role. This could explain the overestimated biomass in our model without iron limitation. Underestimated plankton concentrations in the subtropical gyres are most likely related to insufficient nutrient recycling in the upper ocean. This will be discussed further in sections 3.5 and 4. Another possible reason for differences between the model and the observations is the assumption of a constant chlorophyll to phytoplankton ratio.

[27] Surface nutrient concentrations are also broadly consistent with observations (Figure 8). The model underestimates the nitrate content in the upwelling regions of the eastern tropical Pacific, along the west coast of Africa, and in the northern Indian Ocean. Most of these problems are associated with too fast nutrient uptake by phytoplankton and can be ameliorated by reducing the maximum growth rate as demonstrated by Schmittner and Oschlies (manuscript in preparation, 2005). In the tropical Pacific, the neglect of iron limitation in the model possibly leads to further excessive consumption of nitrate. Along the west coast of North Africa and along the California current, zonal thermocline tilts (not shown) are too small, suggesting that simulated upwelling is too weak. This is a common problem in coarse resolution models [e.g., *Aumont et al.*, 2003].

[28] In the Southern Ocean, simulated nitrate levels are too low north of 55°S and too high south of 65°S such that

Figure 8. Annual mean distribution of nitrate averaged over the top 100 m. (top) Observations from *Conkright et al.* [1998]. (bottom) Model REF at year 2000.
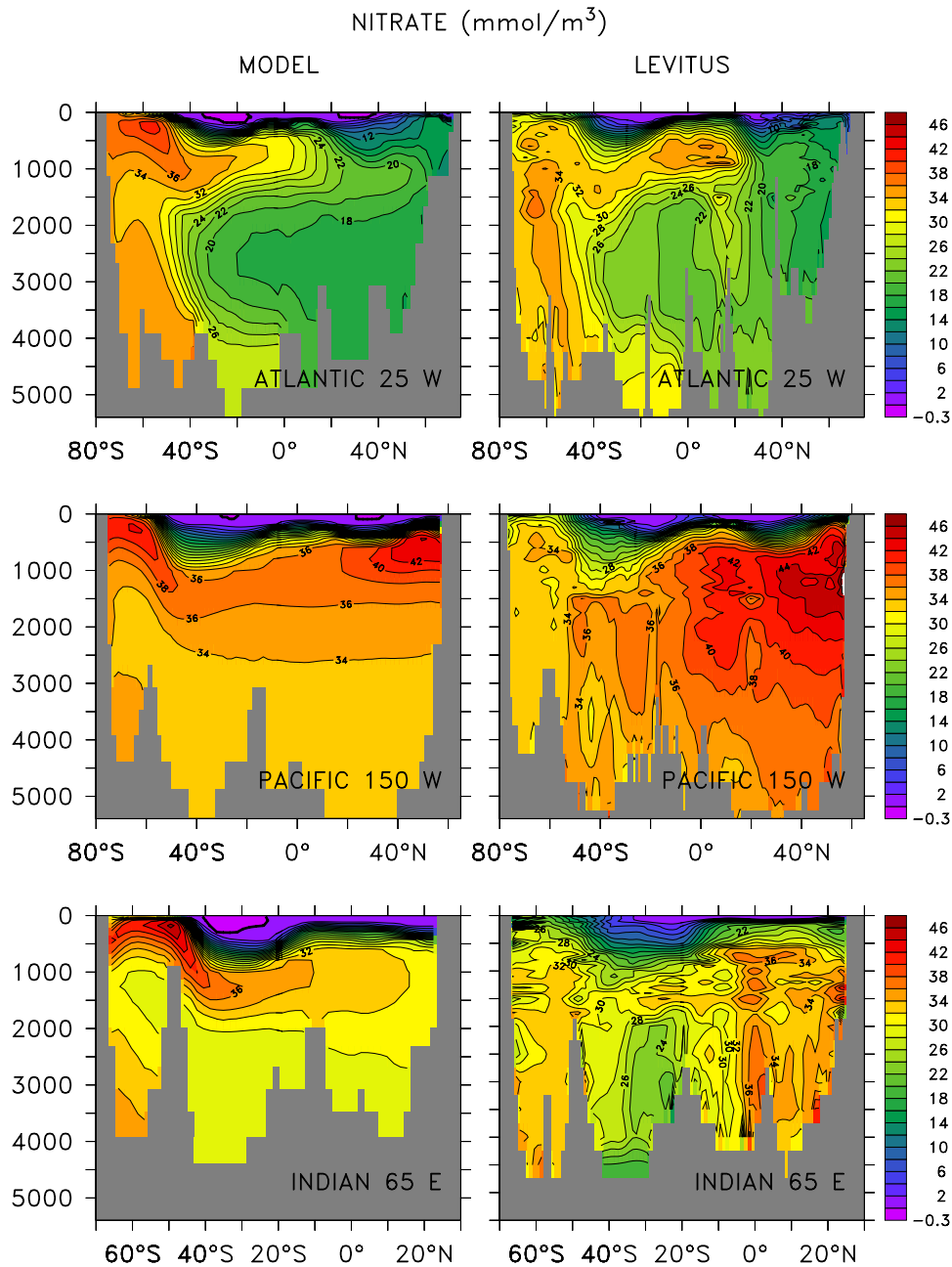
Figure 9. Depth-latitude sections of nitrate distributions (left) simulated by the model REF and (right) from observations [*Conkright et al.*, 1998].

stratification and too shallow remineralization of organic matter.

3.3. Influence of Ocean Mixing

[30] Figure 10 illustrates global measures of model performance for the nitrate distribution. It appears that the best agreement with the observations is obtained for intermediate values of mixing in the pycnocline ($0.2-0.3 \times 10^{-4}$ m^2 s^{-1}). Both larger and smaller values increase the model error.

[31] Models with higher vertical diffusion show a shallower nutricline (Figure 11) and vice versa. This counter-

intuitive response can be understood by assuming that the (low latitude) nutricline is determined by a balance between upwelling of nutrient-rich deep waters and downward diffusion of low nutrient surface waters. Increasing vertical diffusion not only increases the downward diffusion but also increases upwelling (e.g., Table 1). This suggests that changes in upwelling dominate over diffusion in setting the nutricline for different vertical diffusivities.

[32] Surface phytoplankton concentrations respond highly sensitively to changes in vertical mixing (Figure 12). The high mixing case ($K_v = 0.6-1.6$) leads to considerably overestimated concentrations in the tropics, while in the
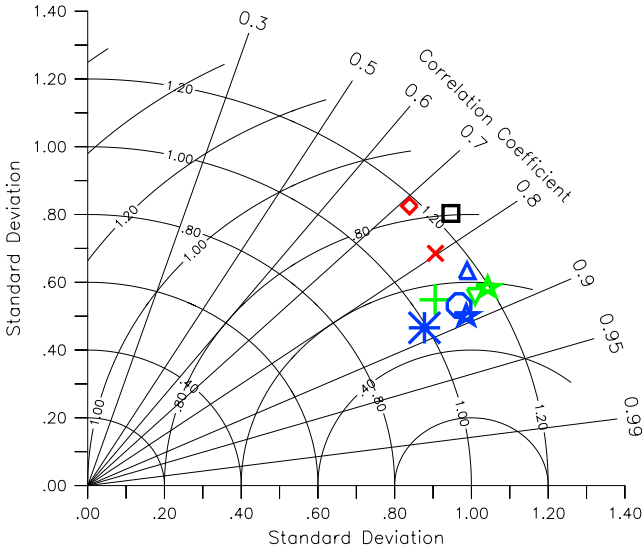
Figure 10. Taylor diagram of simulated annual mean nitrate distributions with respect to observations from *Conkright et al.* [1998]. See Figure 2 for an explanation of the diagram. Black square, tidal $K_b = 0$; blue circle, tidal $K_b = 0.2$; blue triangle base down, tidal $K_b = 0.2$ $A_I = 1000$; blue asterisk, tidal $K_b = 0.2$ $\sigma_{DOM} = 0.25$, $\mu_{DOM} = 0.5$; blue star, REF; green plus, $K_v = 0.3-1.3$; green triangle base up, $K_v = 0.3-1.3$ $w_d = 5-50$; green star, $K_v = 0.3-1.3$ $w_d = 10$; red cross, $K_v = 0.6-1.6$; red diamond, $K_v = 0.6-1.6$ $w_d = 3.5$. Note that colors denote the vertical mixing parameterizations. Red denotes high mixing, blue and green denote intermediate mixing, and black denotes low mixing. Best agreement with the observations shows intermediate diffusivities of around $0.2-0.3$ m^2 s^{-1}.

low mixing case (tidal $K_b = 0$) plankton stocks at low latitudes are too small. Increasing vertical mixing in the Southern Ocean has only small effects on the nutrient distribution (not shown). As for the comparison with temperature, salinity, and nitrate observations, we consistently conclude that intermediate mixing leads to the best agreement with observation based chlorophyll estimates. Note that the high chlorophyll values at high latitudes in the satellite estimates are probably not very reliable, as they might be biased toward summer and good weather conditions. We also reiterate the uncertainties associated with the conversion of phytoplankton biomass to chlorophyll as a potential difficulty in the model data comparison.

[33] The models with high vertical diffusion exhibit strong nutrient trapping in the eastern equatorial Pacific (Figure 13). Nutrient trapping, the positive feedback between upwelling of nutrient-rich deep water, high productivity, and the strong sinking and remineralization of detritus [*Najjar et al.*, 1992], is an artifact observed in many coarse resolution models [*Bacastow and Maier-Reimer*, 1991; *Najjar et al.*, 1992; *Yamanaka and Tajika*, 1997; *Marchal et al.*, 1998]. Here we confirm the findings from studies which show the importance of the circulation [*Aumont et al.*, 1999; *Oschlies*, 2000; *Gnanadesikan et al.*, 2002]. Model $K_v = 0.6-1.6$ shows nitrate concentrations in excess of 100 mmol/m^3 at subsurface levels. No subsurface nitrate maximum is seen in the observations. In model tidal $K_b = 0.2$, nutrient trapping is almost removed, whereas model tidal $K_b = 0$ produces too small subsurface nutrient values. Also interesting is the role of isopycnal mixing in reducing nutrient trapping as can be seen from a comparison of model tidal $K_b = 0.2$ and tidal $K_b = 0.2$ $A_I = 1000$. The reduction of isopycnal diffusion leads to much stronger nutrient trapping. This implies that isopycnal diffusion plays an important role in exporting nutrients from the areas of high
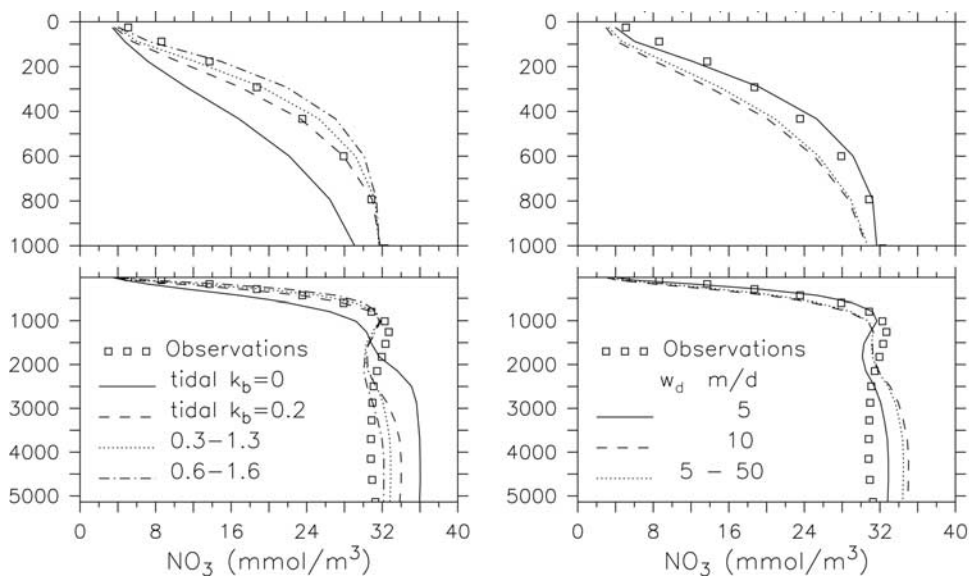

Figure 11. Horizontally averaged nitrate concentrations for experiments (left) with different vertical mixing ($w_d = 5$) and (right) with different sinking speeds ($K_v = 0.3-1.3$).
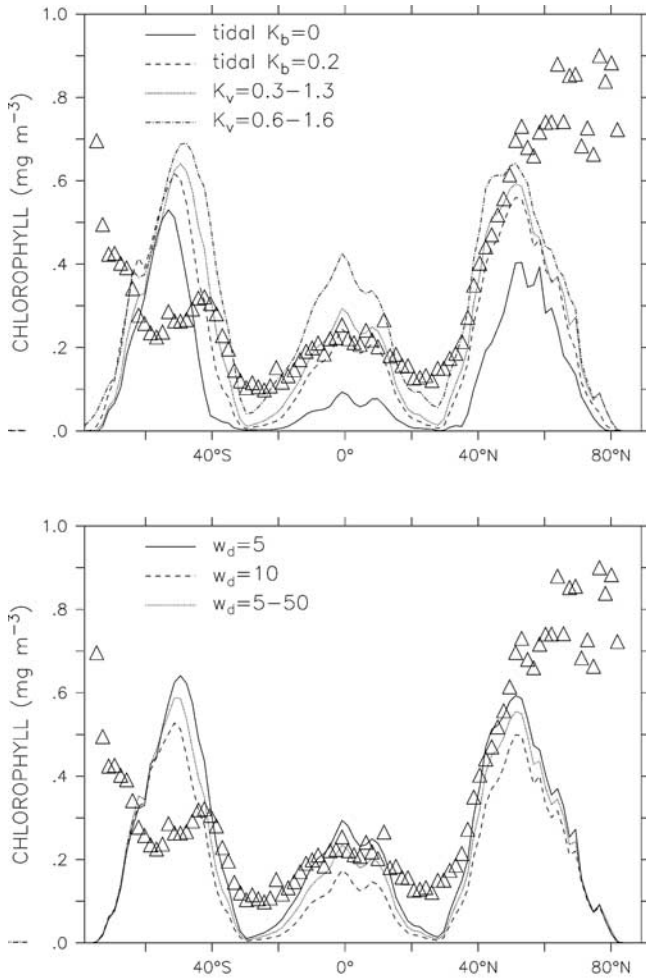
Figure 12. Zonally averaged chlorophyll concentrations for experiments (left) with different vertical mixing ($w_d = 5$) and (right) with different sinking speeds ($K_v = 0.3-1.3$). Symbols denote the SeaWiFS satellite estimates. In order to remove very high and probably false near-coastal data points, a three-point smoother has been applied and values above 1 mg Chl have been removed.

production. This could also explain why the nutrient distribution responds more sensitively to changes in along-isopycnal mixing than temperature or salinity (compare Figure 2 with Figure 10).

3.4. Influence of Particle Sinking and Remineralization

[34] Nutrient trapping can also be substantially reduced by increasing the sinking speed of detritus w_D from 5 to 10 m/d. This is consistent with earlier results by *Yamanaka and Tajika* [1996]. Surface detritus concentrations in the eastern equatorial Pacific are extremely sensitive to changes in w_D. Model $K_v = 0.3-1.3$ with $w_D = 5$ m/d has mean surface concentrations of more than 1 mmol/m^3, while doubling the sinking speed (model $w_D = 10$) decreases the detritus concentrations by one order of magnitude to values smaller than 0.1 mmol/m^3. As the export production is directly

proportional to the detritus concentration, this explains the sensitivity of nutrient trapping to the sinking speed.

[35] Higher sinking speeds of detritus lead to a deepening of the nutricline (Figure 11). This result could be expected, as more efficient export of organic matter leads to a stronger depletion of nutrients in the upper ocean. The model with increasing sinking speed from 5 m/d at 50 m depth to 50 m/d at 5000 m depth ($w_D = 5-50$) shows very similar nutrient profiles and values for global export production (Table 1) as the model with a constant 10-m sinking speed. This result suggests that the increase of particle settling rates with depth as inferred from sediment trap data [*Berelson*, 2002] is neither of major importance for the global nutrient distribution nor for the export of particulate organic matter out of the euphotic zone and that the sinking speed around 300 m depth determines these two variables to a large extent.

[36] The sensitivity of surface plankton concentrations to changes in sinking speed is less than that for mixing
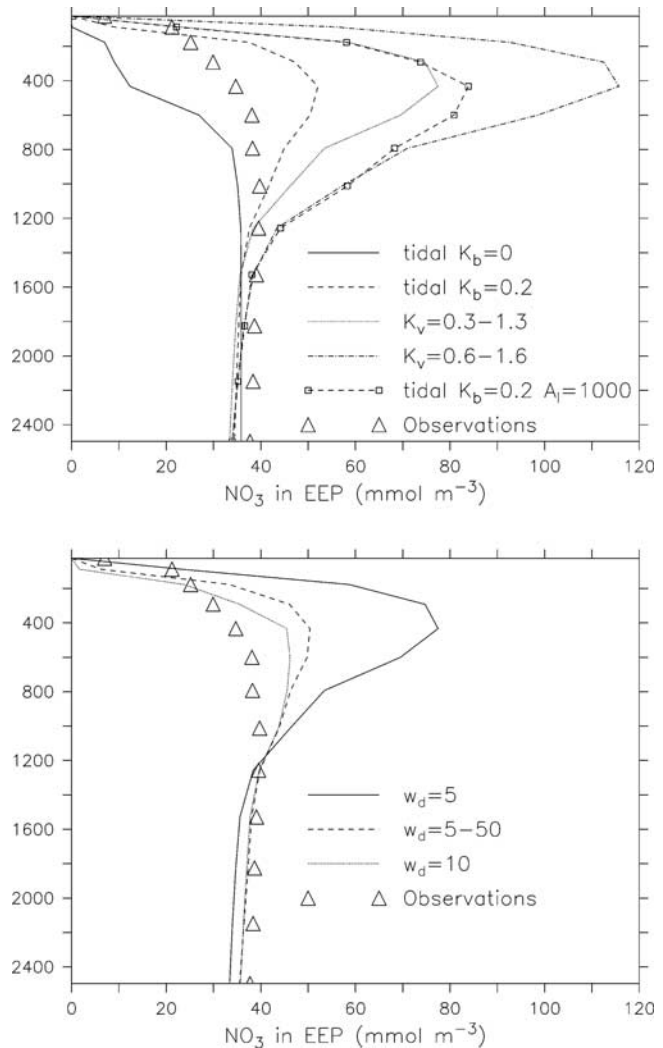

Figure 13. Horizontally averaged nitrate concentrations in the eastern equatorial Pacific (100°W:80°W, 5°S:10°N) for models (left) with different mixing ($w_d = 5$) and (right) with different sinking speeds ($K_v = 0.3-1.3$).
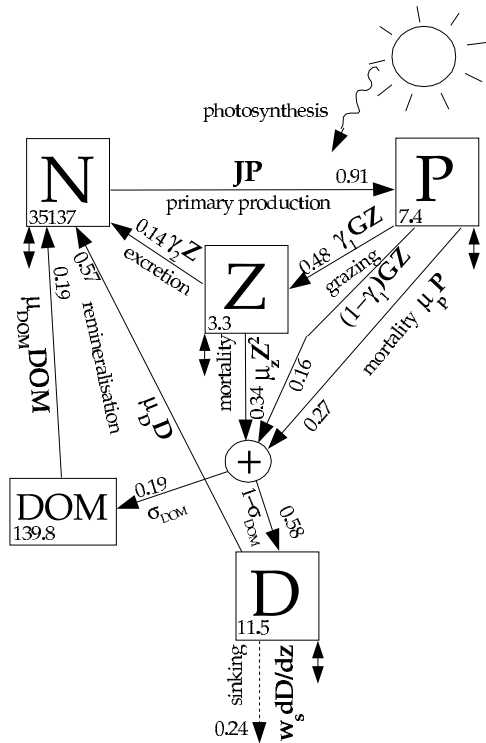
Figure 14. As in Figure 6 but for model tidal $K_b = 0.2$, $\sigma_{DOM} = 0.25$, and $\mu_{DOM} = 0.5$ including cycling of dissolved organic matter.

(Figure 12). Values of w_D around 5 m/d near the surface lead to the best agreement with the observations. Increasing the sinking speed to 10 m/d causes too small plankton concentrations, particularly at low latitudes. Although export production and nutrient profiles for models $w_D = 10$ and $w_D = 5-50$ are very similar, the surface phytoplankton concentrations (Figure 12) and primary productivity (Table 1) are considerably higher in model $w_D = 5-50$, indicating a higher sensitivity of the latter two variables to the sinking speed near the surface.

[37] Note that for constant sinking speeds and remineralization rates, the downward flux of detritus is approximately exponentially decreasing with an e-folding depth of $z_{1/e} = w_D/\mu_D$. Thus, increasing the sinking speed by a factor of 2 is equivalent to decreasing the remineralization rate by one half. This was confirmed by additional model runs not shown here. Nevertheless, an exponential decrease with $z_{1/e} = 100-200$ m is not consistent with measurements of organic particle fluxes [*Martin et al.*, 1987] which show that a considerable amount of particulate matter leaving the euphotic zone enters the deep ocean (5–10% arrives at 2 km depth). Model $w_D = 5-50$ leads to a somewhat slower decline of particle fluxes with depth than the models with a constant sinking speed. However, fluxes into the deep ocean are still too small, and the effect on nutrient distributions is minor (Figures 10 and 11).

3.5. Influence of Dissolved Organic Matter Cycling

[38] Measurements show that a considerable fraction of organic matter in the ocean occurs in dissolved form

[*Hansell*, 2002]. It has been suggested that the cycling of semilabile DOM with a decay time on the order of months to years plays an important role in the surface biogeochemical cycles, while the labile and refractory DOM pools with decay times of minutes to days and hundreds to thousands of years, respectively, are not important [*Yamanaka and Tajika*, 1997]. However, DOM is produced through different and complicated processes, and its production as well as decay rates are not well known [*Carlson*, 2002].

[39] Here we ask the question whether semilabile DOM needs to be included in our marine ecosystem model as an additional tracer. As a criterion, we will use the simulated nutrient and plankton distributions. If inclusion of DOM leads to an improved agreement with the observations, the benefits must be traded against the increased use of computer resources. If this is not the case, the effect of DOM can be regarded as minor and the computational needs of an additional tracer will not generally be warranted.

[40] We have implemented DOM such that a fraction (σ_{DOM}) of the source terms for detritus enters the DOM pool (Figure 14) similar to the approach taken by OCMIP [*Orr et al.*, 2001]. In OCMIP, two thirds of the export production is converted to DOM. In our model, about 40% of the amount of nitrogen entering the detritus pool is exported below 126 m (Figure 6). From this we get a first estimate for $\sigma_{DOM} = 0.25$. Additionally, we performed sensitivity experiments with a lower production ratio ($\sigma_{DOM} = 0.15$). We further assume that DOM remineralizes slower than the particulate detritus pool and that it does not experience sinking. For the remineralization rate μ_{DOM}, we use values of 0.5 yr^{-1} and 0.17 yr^{-1} leading to decay times of 2 and 6 years, respectively.

[41] Including DOM increases the nutrient recycling within the upper ocean. Primary production increases by 15–30% and global phytoplankton and zooplankton biomass increase by 30–50% whereas export through sinking of particles stays almost constant (Table 1, Figure 14). Phytoplankton concentrations increase everywhere except at high latitudes north and south of about 50° (Figure 15). While higher values in the subtropics improve the agreement with the observations, agreement in the tropics becomes worse. Models with large production ratios ($\sigma_{DOM} = 0.25$) overestimate tropical plankton concentrations considerably. Increasing the decay time decreases the gradient between tropical and subtropical plankton concentrations, as nutrients are transported in the form of DOM out of the areas of high production into the oligotrophic gyres. As this gradient was overestimated in the simulation without DOM, this aspect of the plankton distribution seems to be improved. Overall, the plankton simulation is best for the model with a low production ratio ($\sigma_{DOM} = 0.15$) and a long decay time (i.e., low remineralization rate $\mu_{DOM} = 0.17$ yr^{-1}).

[42] Cycling of DOM increases nitrate concentrations in the upper ocean, while concentrations in the deep ocean decrease (Figure 16). The degree of the vertical redistribution is relatively insensitive to the parameter choice. DOM cycling decreases the deviations from the observations in the upper few hundred meters of the ocean and below about 3 km depth whereas at intermediate levels the model error
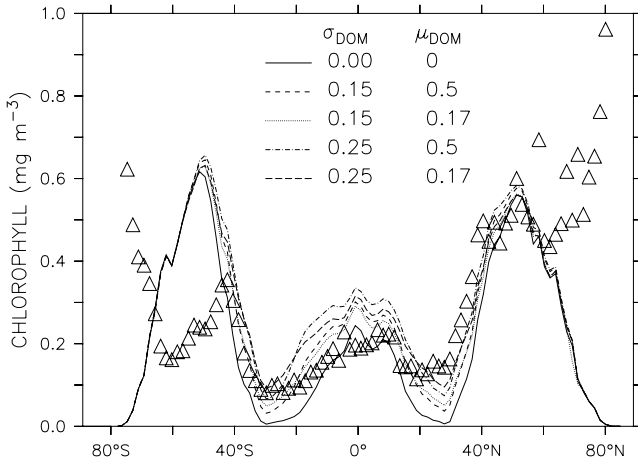
Figure 15. As in Figure 12 but for models including DOM with different production ratios (σ_{DOM}) and remineralization rates (μ_{DOM}).

increases. Thus DOM cycling does not lead to a general improvement of the vertical nitrate distribution.

[43] In contrast to previous simulations with nutrient restoring at the surface [*Bacastow and Maier-Reimer*, 1991; *Najjar et al.*, 1992; *Anderson and Sarmiento*, 1995; *Yamanaka and Tajika*, 1997; *Marchal et al.*, 1998], including DOM in our model has no large effect on nutrient trapping, as vertical profiles in the eastern equatorial Pacific are not influenced much (not shown). As shown above, nutrient trapping is much more controlled by mixing and the treatment of sinking/remineralization of particulate detritus (Figure 13).

[44] Direct measurements of dissolved organic carbon (DOC) or nitrogen (DON) can also be used to constrain the parameter space. *Bronk* [2002] reports mean surface values of DON of 5.8 ± 2 μmol/kg and deep ocean concentrations of 3.9 ± 1.8 μmol/kg. The deep ocean concentration can be regarded as the refractory DOM pool. Thus the semilabile surface concentrations of DON will be about 1.9 μmol/kg. The models yield 1.2, 2.5, 2.2, and 4.3 μmol/kg for (σ_{DOM}, μ_{DOM}) of (0.15, 0.5), (0.15, 0.17), (0.25, 0.5), and (0.25, 0.17), respectively.

[45] Vertical sections of DOC measurements have been compiled by *Hansell* [2002]. In order to compare DOC measurements with the modeled DON, we use a mean value of DOC/DON = 13.6 although observations show a large range of DOC/DON ratios of 9 to 18 [*Benner*, 2002]. In general, all models agree with the observed decrease with depth within the upper few hundred meters (Figure 17). The model with low production ratio and fast decay time (σ_{DOM}, μ_{DOM}) = (0.15, 0.5) mostly underestimates surface DOC concentrations. In the equatorial upwelling regions the model with high production ratio and slow decay (σ_{DOM}, μ_{DOM}) = (0.25, 0.17) overestimates DOC concentrations considerably. This is likely to be related to the excessive productivity in this model. Overall, in best agreement with the observations is the model with small production ratio and long decay time (σ_{DOM}, μ_{DOM}) = (0.15, 0.17). However, all models suffer from large systematic errors. The main

problems are found in the equatorial Pacific where the observations show higher surface values in the west and lower values in the east [*Hansell*, 2002], whereas all models display the opposite gradient. The models also simulate large DOC concentrations in the Southern Ocean between 60°S and 45°S, a feature not present in the observations. The reason for these discrepancies is presumably the use of a constant remineralization rate, which oversimplifies the action of bacteria in converting DOM to ammonium.

[46] We conclude that the model with a small production ratio and a long decay time (σ_{DOM}, μ_{DOM}) = (0.15, 0.17) is in best agreement with available observations. These values are in conflict with higher production ratios of around 0.25 and shorter decay times of about 0.5 years found in a previous study using surface nutrient restoring but a similar DOM model [*Yamanaka and Tajika*, 1997]. The main reason might be slight differences in the model formulation. While *Yamanaka and Tajika* [1997] assume that all particulate organic matter dissolves into the DOM pool, here we assumed that particulate matter directly remineralizes to dissolved inorganic nutrients. Thus, for the same production ratio and decay time, the model of *Yamanaka and Tajika* [1997] would predict higher DOM concentrations than our model.

[47] The advantage of including such a simple parameterization of DOM in our model is the increase of productivity and plankton biomass in the oligotrophic subtropical gyres. However, overall nitrate distributions are not improved and export production through the sinking of particles is not changed.

4. Summary and Discussion

[48] The suite of experiments in section 2, in which parameters were varied that affect the ocean circulation, like diffusivities and surface buoyancy forcing, demonstrated that a parameter combination could be found (model
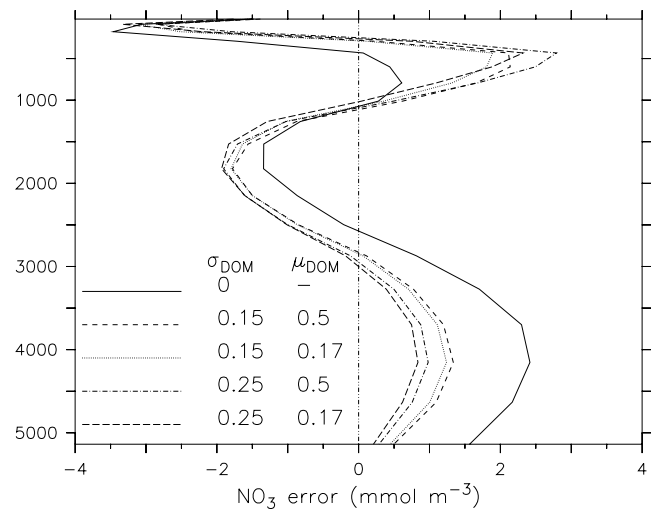

Figure 16. Effect of DOM cycling on vertical nitrate profiles. Plotted is the horizontally averaged error in nitrate fields for model tidal K_b = 0.2 excluding DOM (solid line) and the same model including DOM with different production ratios (σ_{DOM}) and remineralization rates (μ_{DOM}).
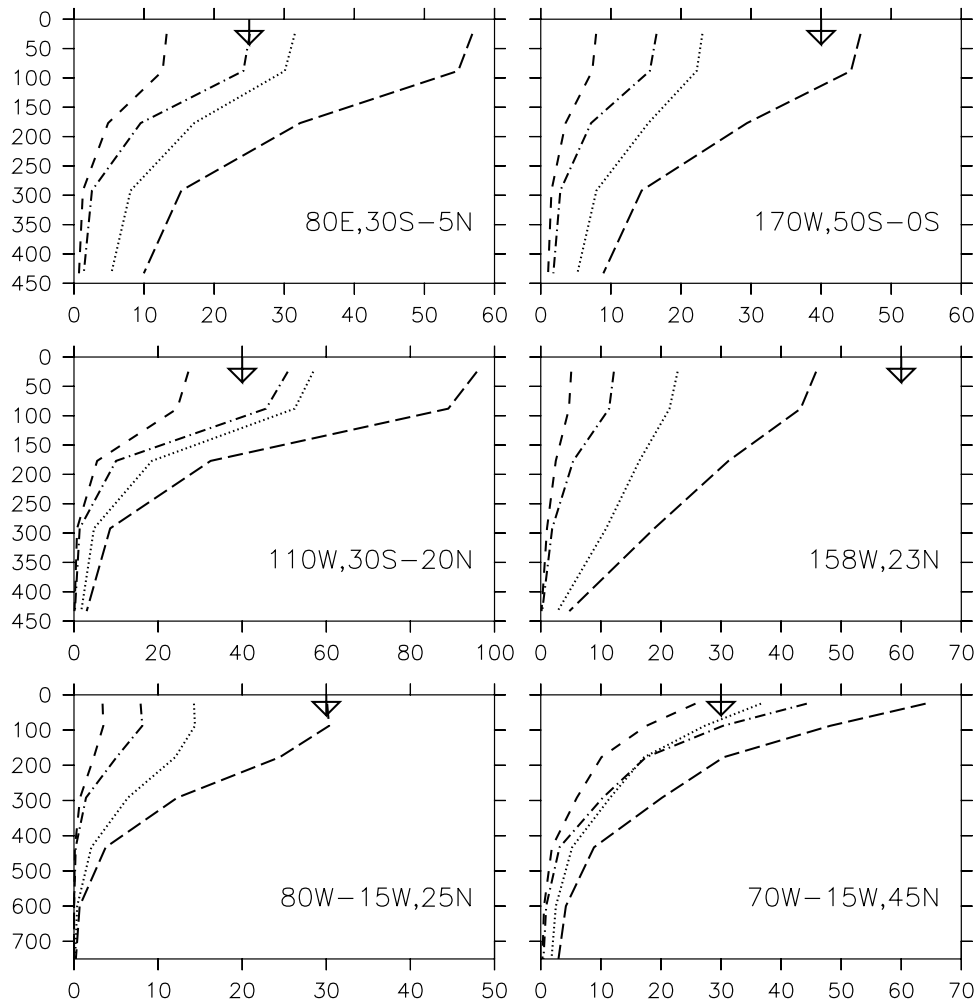
Figure 17. Simulated vertical DOC profiles in μmol/kg from (top left) the Indian Ocean, (top right) the western South Pacific, (middle left) the eastern South Pacific, (middle right) the central North Pacific, and (bottom) the North Atlantic. Vertical axis is depth in meters. The arrow denotes the estimated surface concentration of semilabile DOC from the observations [*Hansell*, 2002]. Therefore we subtracted the concentration of the deep ocean (refractory DOC) from the surface values. The error in the estimation is about 10–30 μmol/kg. The lines denote the different models as in Figures 15 and 16.

REF) such that temperature, salinity, and deep ocean radiocarbon distributions are consistent with observations. These results re-emphasized the role of freshwater forcing in the Southern Ocean and diapycnal mixing in the low-latitude pycnocline in setting the properties and circulation of the global deep water masses. High mixing rates in the deep Southern Ocean (as observed by *Heywood et al.* [2002] and *Naveira-Garabato et al.* [2004]) have a much more limited impact. Although we cannot exclude that other combinations of parameters would be equally consistent with the observations, the agreement with the radiocarbon data strongly supports values for diapycnal diffusion in the pycnocline of around $0.2-0.3 \times 10^{-4}$ m^2 s^{-1}. The only major remaining bias was a too cold deep ocean by about 1°C, which needs further attention in the future.

[49] The reference model as well as all other models with low to intermediate diapycnal mixing predict too low values of primary productivity (see Table 1). As the model does not include the fast recycling pool of ammonia, modeled primary production is only part of primary production in the real ocean. Including a simple model of DOM leads to higher recycling of nutrients in the upper ocean, increases the nutrient delivery to and productivity within the oligotrophic centers of the subtropical gyres, sharpens the nutricline (Figure 16), and thus increases global primary production (Table 1). However, the DOM model in best agreement with chlorophyll and DOM observations increases global primary production by only 16% to 24 Gt C yr^{-1}, which is still considerably lower than observational estimates of 36–57 Gt C yr^{-1} [*Antoine et al.*, 1996; *Morel and Antoine*, 2002; *Falkowski et al.*, 2003; *Gregg et al.*, 2003]. Thus, accounting for fast nutrient recycling, either through direct simulation of ammonium and bacteria as in the original model of *Fasham et al.* [1990] or through a parameterization of this loop (for example, with an additional loss term from the phytoplankton compartment to the

dissolved nutrient pool like in the models of *Six and Maier-Reimer* [1996] and *Schartau and Oschlies* [2003]) will be a priority of future model development (Schmittner and Oschlies, manuscript in preparation, 2005). Difficulties in simulating the observed DOM distribution might also be related to the missing bacterial loop as bacteria are converting DOM into nutrients (ammonium) [e.g., *Spitz et al.*, 2001]. Using a constant remineralization rate seems to oversimplify this process. An alternative approach might be to use a remineralization rate which depends on nitrate (like in the model of *Six and Maier-Reimer* [1996]) in order to account for nutrient limitation of bacteria.

[50] The distribution of nutrients depends on the circulation, and thus mixing and buoyancy and wind forcing, as well as on the biology. For the present combination of the circulation and ecosystem model (REF) a ratio of sinking speed to remineralization rates of 100–200 m yields vertical nutrient distributions consistent with observations. Nevertheless, constant values for sinking velocity and remineralization rates underestimate the particulate organic matter flux into the deep ocean leading to too low nitrate concentrations in the deep North Pacific. Improvements of the particulate matter sinking/remineralization component will be another priority for future model development. In particular, accounting for temperature-dependent remineralization as in the work by *Schartau and Oschlies* [2003] and variable sinking speed, for example, using an aggregate formation model (as in the work of *Ruiz et al.* [2002]) can be expected to lead to further improvements.

[51] The simulated surface nutrient concentrations were generally too low, particularly in the low-latitude upwelling areas like the eastern equatorial Pacific and between 45°S and 50°S in the Southern Ocean. As shown by Schmittner and Oschlies (manuscript in preparation, 2005), these problems are associated with ecosystem model parameters (too fast depletion of upwelled nutrients) and can be improved by decreasing the maximum growth rate for phytoplankton.

[52] Here we have shown that the reference model is consistent with temperature, salinity, mixed layer depth, and deep ocean radiocarbon, as well as nitrate and chlorophyll observations. Increased vertical mixing leads to a sharper nutricline due to intensified upwelling. Nutrient trapping in the eastern equatorial Pacific is strongly dependent on diapycnal as well as on isopycnal diffusion and on the parameterization of vertical particulate matter fluxes (i.e., sinking/remineralization) but not on the inclusion of DOM cycling. The latter result is in contrast to and calls into question previous studies using surface nutrient restoring [*Bacastow and Maier-Reimer*, 1991; *Najjar et al.*, 1992; *Anderson and Sarmiento*, 1995; *Yamanaka and Tajika*, 1997; *Marchal et al.*, 1998].

5. Conclusions

[53] A new model of the upper ocean ecosystem has been interactively coupled into the three-dimensional ocean circulation component of a coupled Earth System Climate Model. We have shown that the model successfully reproduces many features of present-day distributions of nutrients and phytoplankton as well as temperature, salinity, radiocarbon, and mixed layer depth. The model versions in best agreement with observations have small to intermediate values (0.2–0.3 cm²/s) of vertical mixing in the pycnocline and e-folding depths for particulate organic matter fluxes of 100–200 m. Inclusion of dissolved organic matter increases productivity in the subtropical gyres, improving model performance there. Areas of future model development are the inclusion or parameterization of the fast recycling ammonium/bacteria loop and improvements of the particle sinking/remineralization module. Furthermore, including other limiting nutrients like phosphate, silicate, or iron as well as accounting for different functional plankton groups are possibilities for future model extensions. The model is suitable for multimillenial timescale simulations. It is currently applied to study the effect of rapid changes in ocean circulation during past and future climate change to the marine ecosystem [*Schmittner* 2005] as well as to productivity changes associated with the closure of the Panama isthmus 3 Ma ago (B. Schneider and A. Schmittner, Simulating the impact of the Panamanian seaway closure on ocean circulation, marine productivity and nutrient cycling, manuscript in preparation, 2005). A full marine carbon cycle module is under development. The model will be available for the community via the UVic web site http://climate.uvic.ca/model or by contacting one of the authors.

References

Anderson, L. A., and J. L. Sarmiento (1995), Global ocean phosphate and oxygen simulations, *Global Biogeochem. Cycles*, 9, 621–636.

Antoine, D., J.-M. André, and A. Morel (1996), Oceanic primary production: 2. Estimation at global scale from satellite (coastal zone color scanner) chlorophyll, *Global Biogeochem. Cycles*, 10, 57–69.

Aumont, O., J. C. Orr, P. Monfray, G. Madec, and E. Maier-Reimer (1999), Nutrient trapping in the equatorial Pacific: The ocean circulation solution, *Global Biogeochem. Cycles*, 13, 351–369.

Aumont, O., E. Maier-Reimer, S. Blain, and P. Pondaven (2003), An ecosystem model of the global ocean including Fe, Si, P co-limitations, *Global Biogeochem. Cycles*, 17(2), 1060, doi:10.1029/2001GB001745.

Bacastow, B., and E. Maier-Reimer (1991), Dissolved organic carbon in modelling oceanic new production, *Global Biogeochem. Cycles*, 5, 71–85.

Benner, R. (2002), Chemical composition and reactivity, in *Biogeochemistry of Marine Dissolved Organic Matter*, edited by D. A. Hansell and C. A. Carlson, pp. 59–90, Elsevier, New York.

Berelson, W. M. (2002), Particle settling rates increase with depth in the ocean, *Deep Sea Res., Part II*, 49, 237–251.

Bronk, D. A. (2002), Dynamics of DON, in *Biogeochemistry of Marine Dissolved Organic Matter*, edited by D. A. Hansell and C. A. Carlson, pp. 153–247, Elsevier, New York.

Bryan, K. (1987), Parameter sensitivity of primitive equation ocean general circulation models, *J. Phys. Oceanogr.*, 17, 970–985.

Bryan, K., and L. J. Lewis (1979), A water mass model of the world oceans, *J. Geophys. Res.*, 84, 2503–2517.

Carlson, C. A. (2002), Production and removal processes, in *Biogeochemistry of Marine Dissolved Organic Matter*, edited by D. A. Hansell and C. A. Carlson, pp. 91–151, Elsevier, New York.

Conkright, M. E., S. Levitus, T. O'Brien, T. Boyer, J. Antonov, and C. Stephens (1998), *World Ocean Atlas 1998*, *Tech. Rep. 15*, NOAA Natl. Oceanogr. Data Cent., Silver Spring, MD.

Denman, K. L. (2003), Modelling planktic ecosystems: Parameterizing complexity, *Prog. Oceanogr.*, 57, 429–452.

Evans, G. T., and V. C. Garçon (1995), One-dimensional models of water column biogeochemistry, technical report, Joint Global Ocean Flux Study, Paris.

Evans, G. T., and J. S. Parslow (1985), A model of annual plankton cycles, *Biol. Oceanogr.*, *3*, 328–347.

Falkowski, P. G., E. A. Laws, R. T. Barber, and J. W. Murray (2003), Phytoplankton and their role in primary, new, and export production, in *Ocean Biogeochemistry*, edited by M. J. R. Fasham, chap. 4, pp. 99–121, Springer, New York.

Fasham, M. J. R., H. W. Ducklow, and S. M. McKelvie (1990), A nitrogen-based model of plankton dynamics in the oceanic mixed layer, *J. Mar. Res.*, *48*, 591–639.

Ganachaud, A., and C. Wunsch (2000), Improved estimates of global ocean circulation, heat transport and mixing from hydrographic data, *Nature*, *408*, 453–456.

Gent, P. R., and J. C. McWilliams (1990), Isopycnal mixing in ocean circulation models, *J. Phys. Oceanogr.*, *20*, 150–155.

Gerdes, R., C. Koeberle, and J. Willebrandt (1991), The influence of numerical advection schemes on the results of ocean general circulation models, *Clim. Dyn.*, *5*, 211–226.

Gnanadesikan, A., R. D. Slater, N. Gruber, and J. L. Sarmiento (2002), Ocean vertical exchange and new production: A comparison between models and observations, *Deep Sea Res., Part II*, *49*, 363–401.

Gnanadesikan, A., J. P. Dunne, R. M. Key, K. Matsumoto, J. L. Sarmiento, R. D. Slater, and P. S. Swathi (2004), Oceanic ventilation and biogeochemical cycling: Understanding the physical mechanisms that produce realistic distributions of tracers and productivity, *Global Biogeochem. Cycles*, *18*, GB4010, doi:10.1029/2003GB002097.

Gregg, W. W., M. E. Conkright, P. Ginoux, J. E. O'Reilly, and N. W. Casey (2003), Ocean primary production and climate: Global decadal changes, *Geophys. Res. Lett.*, *30*(15), 1809, doi:10.1029/2003GL016889.

Halpern, D., et al. (2003), Live access to US JGOFS SMP data: Monthly mean global surface ocean variables, http://usjgofs.whoi.edu/las/servlets/dataset, U.S. Joint Global Ocean Flux Study, Woods Hole, Mass.

Hansell, D. A. (2002), DOC in the global ocean carbon cycle, in *Biogeochemistry of Marine Dissolved Organic Matter*, edited by D. A. Hansell and C. A. Carlson, pp. 685–715, Elsevier, New York.

Heywood, K., A. C. Naveira Garabato, and D. P. Stevens (2002), High mixing rates in the abyssal Southern Ocean, *Nature*, *415*, 1011–1014.

Jayne, S. R., and L. C. St. Laurent (2001), Parameterizing tidal dissipation over rough topography, *Geophys. Res. Lett.*, *28*, 811–814.

Ledwell, J. R., A. J. Watson, and C. S. Law (1994), Evidence for slow mixing across the pycnocline from an open-ocean tracer release experiment, *Nature*, *364*, 701–703.

Levitus, S., and T. P. Boyer (1994), *World Ocean Atlas 1994, vol. 4, Temperature*, NOAA Atlas NESDIS 4, 117 pp., Natl. Oceanic and Atmos. Admin., Silver Spring, Md.

Levitus, S., R. Burgett, and T. P. Boyer (1994), *World Ocean Atlas 1994, vol. 3, Salinity*, NOAA Atlas NESDIS 3, 99 pp., Natl. Oceanic and Atmos. Admin., Silver Spring, Md.

Marchal, O., T. F. Stocker, and F. Joos (1998), A latitude-depth, circulation-biogeochemical ocean model for paleoclimate studies: Development and sensitivities, *Tellus, Ser. B*, *50*, 290–316.

Martin, J. H., G. A. Knauer, D. M. Karl, and W. W. Broenkow (1987), VERTEX: Carbon cycling in the northeast Pacific, *Deep Sea Res.*, *34*, 267–285.

Matsumoto, K., et al. (2004), Evaluation of ocean carbon cycle models with data-based metrics, *Geophys. Res. Lett.*, *31*, L07303, doi:10.1029/2003GL018970.

Monterey, G., and S. Levitus (1997), *Seasonal Variability of Mixed Layer Depth for the World Ocean*, NOAA Atlas NESDIS 14, 96 pp., Natl. Oceanic and Atmos. Admin., Silver Spring, Md.

Moore, J. K., S. C. Doney, J. A. Kleypas, D. M. Glover, and I. Y. Fung (2002), An intermediate complexity marine ecosystem model for the global domain, *Deep Sea Res., Part II*, *49*, 403–462.

Morel, A., and D. Antoine (2002), Small critters–big effects, *Science*, *296*, 1980–1982.

Najjar, R. G., J. L. Sarmiento, and J. R. Toggweiler (1992), Downward transport and fate of organic matter in the ocean: Simulations with a general circulation model, *Global Biogeochem. Cycles*, *6*, 45–76.

Naveira-Garabato, A. C., K. L. Polzin, B. A. King, K. J. Heywood, and M. Visbeck (2004), Widespread intense turbulent mixing in the Southern Ocean, *Science*, *303*, 210–213.

Orr, J., et al. (2001), Estimates of anthropogenic carbon uptake from four three-dimensional global ocean models, *Global Biogeochem. Cycles*, *15*, 43–60.

Oschlies, A. (2000), Equatorial nutrient trapping in biogeochemical ocean models: The role of advection numerics, *Global Biogeochem. Cycles*, *14*, 655–668.

Oschlies, A. (2001), Model-derived estimates of new production: New results point towards lower values, *Deep Sea Res., Part II*, *48*, 2173–2197.

Oschlies, A., and V. Garçon (1999), An eddy-permitting coupled physical-biological model of the North Atlantic: 1. Sensitivity to advection numerics and mixed layer physics, *Global Biogeochem. Cycles*, *13*, 135–160.

Pacanowski, R. (1995), MOM 2 documentation user's guide and reference manual, technical report, Geophys. Fluid Dyn. Lab. Ocean Group, Princeton, N. J.

Ruiz, J., L. Prieto, and F. Ortegón (2002), Diatom aggregate formation and fluxes: A modeling analysis under different size-resolution schemes and with empirical determined aggregation kernels, *Deep Sea Res., Part I*, *49*, 495–515.

Saenko, O. A., A. J. Weaver, and A. Schmittner (2003), Atlantic deep circulation controlled by freshening in the Southern Ocean, *Geophys. Res. Lett.*, *30*(14), 1754, doi:10.1029/2003GL017681.

Sarmiento, J. L., R. D. Slater, M. J. R. Fasham, H. W. Ducklow, J. R. Toggweiler, and G. T. Evans (1993), A seasonal three-dimensional ecosystem model of nitrogen cycling in the North Atlantic euphotic zone, *Global Biogeochem. Cycles*, *7*, 417–450.

Schartau, M., and A. Oschlies (2003), Simultaneous data-based optimization of a 1d-ecosystem model at three locations in the North Atlantic: I. Method and parameter estimates, *J. Mar. Res.*, *61*, 765–793.

Schmittner, A. (2005), Decline of the marine ecosystem caused by a reduction in the Atlantic overturning circulation, *Nature*, *443*, 628–633.

Shirasawa, K., M. Leppäranta, J. Ehn, M. Granskog, N. Ishikawa, and T. Kawamura (2001), Ice and snow cover as a filter of solar radiation in natural waters, in *Current Problems in Optics of Natural Waters*, edited by I. Levin and G. Gilbert, pp. 278–282, D. S. Rozhdestvensky Opt. Soc., St. Petersburg, Russia.

Simmons, H. L., S. R. Jayne, L. C. St. Laurent, and A. J. Weaver (2004), Tidally driven mixing in a numerical model of the ocean general circulation, *Ocean Modell.*, *6*, 245–263.

Six, K. D., and E. Maier-Reimer (1996), Effects of plankton dynamics on seasonal carbon fluxes in an ocean general circulation model, *Global Biogeochem. Cycles*, *10*, 559–584.

Spitz, Y. H., J. R. Moisan, and M. R. Abbott (2001), Configuring an ecosystem model using data from the Bermuda Atlantic Time Series (BATS), *Deep Sea Res., Part II*, *48*, 1733–1768.

St. Laurent, L., H. Simmons, and S. Jayne (2002), Estimating tidally driven mixing in the deep ocean, *Geophys. Res. Lett.*, *29*(23), 2106, doi:10.1029/2002GL015633.

Suess, E. (1980), Particulate organic carbon flux in the oceans—Surface productivity and oxygen utilization, *Nature*, *288*, 260–263.

Taylor, K. E. (2001), Summaring multiple aspects of model performance in a single diagram, *J. Geophys. Res.*, *106*, 7183–7192.

Toggweiler, J. R., K. Dixon, and K. Bryan (1989), Simulation of radiocarbon in a coarse-resolution world ocean model: 2. Distributions of bomb-produced carbon 14, *J. Geophys. Res.*, *94*, 8243–8264.

Weaver, A. J., et al. (2001), The UVic Earth System Climate Model: Model description, climatology, and applications to past, present and future climates, *Atmos. Ocean*, *39*(4), 361–428.

Yamanaka, Y., and E. Tajika (1996), The role of vertical fluxes of particulate organic matter and calcite in the oceanic carbon cycle: Studies using an ocean biogeochemical general circulation model, *Global Biogeochem. Cycles*, *10*, 361–382.

Yamanaka, Y., and E. Tajika (1997), Role of dissolved organic matter in the marine biogeochemical cycle: Studies using an ocean biogeochemical general circulation model, *Global Biogeochem. Cycles*, *11*, 599–612.

————————————

M. Eby, School for Earth and Ocean Sciences, University of Victoria, PO Box 3055, Victoria, BC V8W 3P6, Canada. (eby@uvic.ca)

X. Giraud, Research Center on Ocean Margins, University of Bremen, FB5, Postfach 330440, D-28334 Bremen, Germany. (xgiraud@palmod.uni-bremen.de)

A. Oschlies, School of Ocean and Earth Science, Southampton Oceanography Centre, Southampton SO14 3ZH, UK. (andreas.oschlies@soc.soton.ac.uk)

A. Schmittner, College of Oceanic and Atmospheric Sciences, Oregon State University, 104 Ocean Administration Building, Corvallis OR 97331, USA. (aschmittner@coas.oregonstate.edu)

H. L. Simmons, International Arctic Research Center, University of Alaska, Fairbanks, 903 Koyukuk Drive, Fairbanks, AK 99775-7340, USA. (hsimmons@iarc.uaf.edu)